2018

Field-scale multi-phase LNAPL remediation: Validating a new computational framework against sequential field pilot trials

Kaveh Sookhak Lari
Edith Cowan University

Colin Johnson

John Rayner

Greg Davis

10.1016/j.jhazmat.2017.11.006
Sookhak Lari, K., Johnston, C. D., Rayner, J. L., & Davis, G. B. (2018). Field-scale multi-phase LNAPL remediation: Validating a new computational framework against sequential field pilot trials. *Journal of Hazardous Materials, 345*, 87-96. Available here

Journal of Hazardous Materials 345 (2018) 87–96

Contents lists available at ScienceDirect

Journal of Hazardous Materials

journal homepage: www.elsevier.com/locate/jhazmat

Research Paper

Field-scale multi-phase LNAPL remediation: Validating a new computational framework against sequential field pilot trials

Kaveh Sookhak Lari[a,b,c,*], Colin D. Johnston[a,b], John L. Rayner[a,b], Greg B. Davis[a,b,d]

[a] CSIRO Land and Water, Private Bag No. 5, Wembley, WA 6913, Australia
[b] Cooperative Research Centre for Contamination Assessment and Remediation of the Environment (CRC CARE), Australia
[c] School of Engineering, Edith Cowan University, 270 Joondalup Drive, Joondalup, WA 6027,Australia
[d] School of Earth Sciences, The University of Western Australia, 35 Stirling Highway, Crawley,WA 6009, Australia

HIGHLIGHTS

- For the first time, a TMVOC-MP framework modelled multi-phase LNAPL recovery.
- Its multi-component feature allows simultaneous partitioning of various hazardous chemicals.
- For the first time, its field-scale performance on two supercomputers was compared.
- Results were verified using complex LNAPL recovery data from a contaminated site.
- It can define recovery endpoints and long-term risks caused by hazardous materials.

ARTICLE INFO

Article history:
Received 7 June 2017
Received in revised form 22 October 2017
Accepted 3 November 2017
Available online 4 November 2017

Keywords:
LNAPL remediation
Multi-phase
Multi-component
Supercomputing
Risk

ABSTRACT

Remediation of subsurface systems, including groundwater, soil and soil gas, contaminated with light non-aqueous phase liquids (LNAPLs) is challenging. Field-scale pilot trials of multi-phase remediation were undertaken at a site to determine the effectiveness of recovery options. Sequential LNAPL skimming and vacuum-enhanced skimming, with and without water table drawdown were trialled over 78 days; in total extracting over 5 m^3 of LNAPL. For the first time, a multi-component simulation framework (including the multi-phase multi-component code TMVOC-MP and processing codes) was developed and applied to simulate the broad range of multi-phase remediation and recovery methods used in the field trials. This framework was validated against the sequential pilot trials by comparing predicted and measured LNAPL mass removal rates and compositional changes. The framework was tested on both a Cray supercomputer and a cluster. Simulations mimicked trends in LNAPL recovery rates (from 0.14 to 3 mL/s) across all remediation techniques each operating over periods of 4–14 days over the 78 day trial. The code also approximated order of magnitude compositional changes of hazardous chemical concentrations in extracted gas during vacuum-enhanced recovery. The verified framework enables longer term prediction of the effectiveness of remediation approaches allowing better determination of remediation endpoints and long-term risks.

1. Introduction

Accidental release of non-aqueous phase liquids (NAPLs), such as petroleum hydrocarbons, into the subsurface can pose significant health and environmental concerns. These include (but not limited to) exposing the receiving media (soil, soil gas, groundwater and ambient air) to thousands of chemicals, some with high health risk profiles (e.g. carcinogenic compounds) [1,2]. Light NAPLs (LNAPLs) mostly reside in the zone of water table fluctuation and therefore, pose hazards in air (vapour) and water phases [3–6]. The recovery and removal of LNAPLs and mitigation of the risks they pose is a primary step in remediation of contaminated sites. Due to the nature of LNAPLs in the subsurface, several remedial approaches can be used, including air, water or solvent flushing or single, dual and multi-phase purging of LNAPL, soil gas and water [7–10]. However, the effectiveness and success of any (or combination) of these

* Corresponding author at: CSIRO Land and Water, Private Bag No. 5, Wembley, WA, 6913, Australia.
E-mail addresses: kaveh.sookhaklari@csiro.au, kaveh_lari@yahoo.com (K. Sookhak Lari).

https://doi.org/10.1016/j.jhazmat.2017.11.006

approaches for a particular case greatly depends on their feasibility, proper application and subsurface conditions.

In general, any engineering approach such as pilot field-scale trials to determine an appropriate sequence and configuration of the recovery methods for a particular site may be expensive and time consuming. Furthermore, the long-term outcome and the endpoint of LNAPL recovery is not easily predictable by simply extrapolating the results from field-scale trials. Since computational methods can be a powerful tool for dealing with long-term and realistic problems involved in large time and spatial scale geoscience systems [11], representative computational simulation becomes a non-invasive and potentially more affordable technique to elucidate the effectiveness of complex remediation options (e.g. [12,13]) and LNAPL recovery strategies [14]. Validation of such computational methods is a critical first step.

Transport, partitioning and fate of LNAPL in porous media as well as common recovery methods have critical characteristics and features which should be adequately addressed in a representative simulation. First, the combination of the LNAPL plume morphology, location of the recovery wells and the soil heterogeneity and stratification may form a highly asymmetric problem which cannot be dealt with using simplifying assumptions such as symmetric modelling domains [15,16]. Second, the release, transport and partitioning of LNAPL in porous media is a multi-phase (air, water and LNAPL) and multi-component problem. The state of the LNAPL plume over the course of remediation can be very dynamic, with its phase behaviour very much dependent on compositional changes. This also means that LNAPL dissolution fronts can become unstable during their propagation [17].[1] Furthermore, the recovery methods also include complex regimes of multi-phase extraction of liquids and gases from the subsurface. To accommodate all these features, a combined multi-phase and multi-component modelling strategy is needed to represent field conditions [19].

Various multi-phase and multi-component models for simulation of LNAPL movement and partitioning in subsurface systems have been applied over the last decade. An introduction to these models and discussions on the capabilities of each are presented in the literature [20,21]. Among these models, the serial-processing code TMVOC (a member of the TOUGH2 family of codes [22]) has shown its ability to mimic the most critical behaviours of the multi-component LNAPL transport and partitioning for simplified problems [23,24,21,16]. TMVOC is an integral finite-difference numerical code, written in FORTRAN 77, which practically solves discretised partial differential equations governing non-isothermal subsurface transport phenomena at a Darcy-scale. The code includes various options for constitutive relationships, partitioning attributes of the components and biological degradation. The source code is well-structured and therefore, it is possible to amend and modify the code as needed [21]. The parallel version of the code, TMVOC-MP (a member of the TOUGH2-MP group of codes) was also released in 2007 [25]. Generally, TMVOC has not been used for field-scale LNAPL recovery and groundwater remediation problems [26].

Here, we aim to build, test and verify a parallel-processing modelling framework, based on TMVOC-MP, to representatively simulate three dimensional (3D), field-scale application of complex LNAPL recovery and groundwater remediation approaches including multi-phase and multi-component removal of liquids and gases from the subsurface. We investigate the capabilities of such a modelling framework plus its computational costs to conduct representative simulations. The modelling framework is tested on two different supercomputing facilities with different architectures. We discuss the performance of the framework on each facility and also comment on some of the experiences gained during compilation and execution of the code.

To test and verify the framework, we use data from a field scale LNAPL recovery and groundwater remediation study at a site in Western Australia. The field pilot trials included sequential application of various multi-phase LNAPL remedial approaches and the key results are reported here for the first time. The site was contaminated by weathered gasoline/kerosene. Field tests were conducted to map the LNAPL distribution in the subsurface and identify the processes controlling the effectiveness of various LNAPL recovery methods including skimming, vacuum-enhanced recovery, slurping and water table drawdown. The measurements, including the rate and total volume of LNAPL recovered, soil gas pressures and composition of the soil gas were recorded during application of various recovery methods [27,28]. To demonstrate the capabilities of the modelling framework for field-scale 3D representative simulations and to verify the code, we implemented the sequential LNAPL recovery approaches into the framework and compared the simulation results with the field measurements. Due to the nature of the various recovery methods applied, the framework testing and verification spans various levels of the dynamics in the system including short and long temporal and spatial scales.[2]

This is the first validation of a parallel-processing framework that models field-scale, multi-phase and multi-component partitioning processes required to simulate LNAPL product recovery and multi-phase complex subsurface remedial technologies. We briefly discuss critical characteristics and data from the field site, describe the governing equations and the model features, the simulation resources, performance and the results. The capabilities, features and computational costs of this modelling framework (through the presented 3D field-scale simulation) help decide where such modelling can be applied to elucidate the effectiveness of appropriate remediation methods for various site conditions and resources. The ability of this modelling framework in dealing with detailed field-scale problems can be of particular importance for predicting the effective endpoint of expensive subsurface LNAPL remediation processes and in determining the longevity of risks posed by LNAPLs, which is still a challenging task.

2. The field site, remedial approach and key findings

The site under study is located in Western Australia. The site hydrogeology, contamination features and the recovery methods were reported in [27,29,28]. The average maximum and minimum temperatures at the site were 27 and 16 ◦ Celsius respectively. The site altitude is a few meters above sea level. For the period of 1876–2015, the average annual rainfall of the region was 839 *mm* [30]. Cores were collected to determine soil physical properties and the distribution of LNAPL and its components in the profile. Soil gas was sampled from multi-level samplers and air extraction lines.

Results of the core sampling indicated that the soil type is generally fine to coarse sand with some isolated and non-correlated heterogeneities and partially cemented zones. The nominated multi-phase recovery well located almost at the centre of the LNAPL plume is depicted in Fig. 1 (Right). The depth-averaged composition of the LNAPL is reported in Table 1, indicating that it can be characterised as weathered gasoline/kerosene. The average fluid distribution profile at the site is also shown in Fig. 2. Field cores and LNAPL thickness measurements in wells indicated that the LNAPL plume had an approximate radius of 50 m.

[1] Research is currently in progress on this topic [18].

[2] We intentionally kept the 3D layout of the problem to estimate the computational cost for simulating asymmetric field-size problems using similar computational resources.

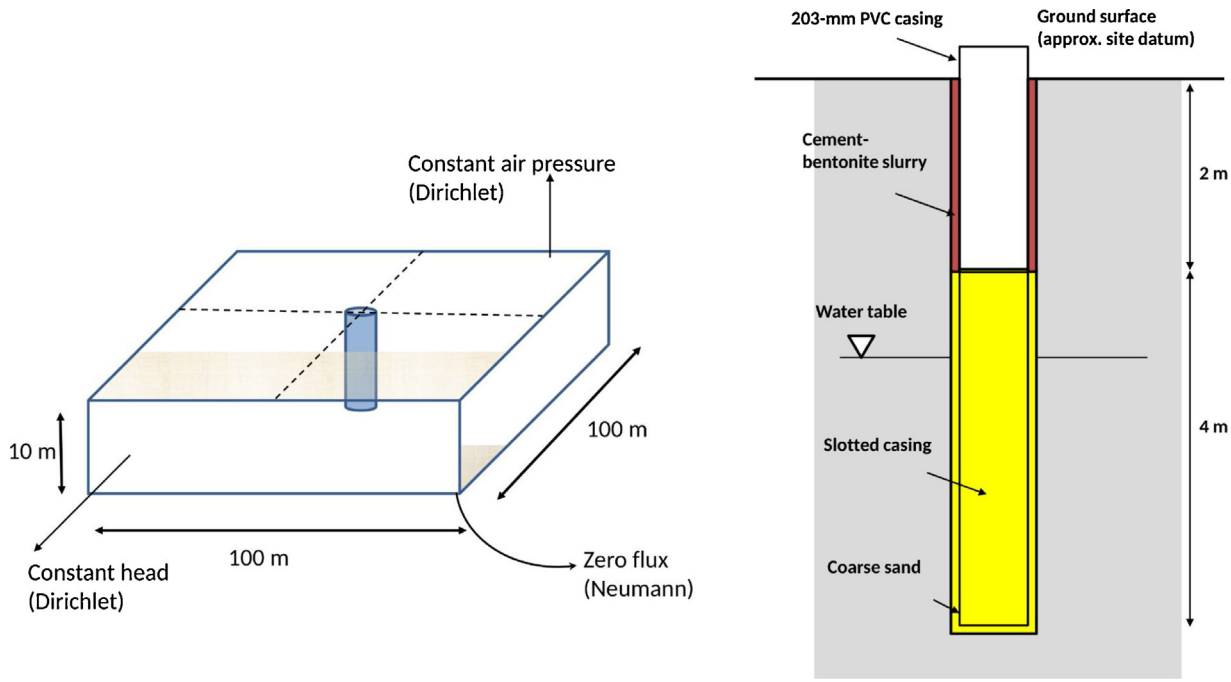

Fig. 1. Left: The simulation domain and the boundary conditions; Right: The recovery well (at the site) configuration.

Table 1
Abundance and properties of compounds found in the LNAPL plume. Data on Wagner equation coefficients is adopted from [31], solubilities S_W from [5], diffusion coefficients D, viscosity μ, molecular weight M_W, critical pressure and temperature (Pc and Tc) from [32] and density ρ from [33]. Xyl is xylene, EtBen is ethylbenzene, Napht is naphthalene and TMB is trimethylbenzene.

	Mass	Mole	M_W	S_W	$10^5 S_W$	$D \times 10^9$		Wagner Eq.				Pc	Tc	μ	ρ	Group
	%	%	g/mole	mg/mole	mole/mole	Aq (m^2/s)	G (m^2/s)	α_1	α_2	α_3	α_4	atm	C	cp	kg/m^3	
Benzene	0.029	0.062	78.11	1762.2	40.60	1.16	9350	−6.94739	1.25253	−2.53686	−3.49284	48.96	562.10	0.606	873	BEN
Toluene	0.001	0.002	92.14	547.1	10.69	0.97	8520	−7.28607	1.38091	−2.83433	−2.79168	41.06	591.72	0.553	861	TOL
m/p-Xyl	0.353	0.557	106.16	171.7	2.91	0.8	6820	7.613585	1.450825	−3.21212	−2.59543	35.20	616.50	0.603	856	XYL
o-Xyl	0.022	0.0650	106.16	172	2.92	0.79	7300	−7.53357	1.40968	−3.10985	−2.85992	37.32	630.25	0.747	875	
EtBen	0.223	0.350	106.17	184.3	3.12	0.92	7580	−7.48645	1.45488	−3.37538	−2.23048	36.02	617.12	0.629	867	ETB
135TMB	0.287	0.200	240.35	48.2	0.36	0.74	6770	−8.37150	2.41166	−5.30321	2.67635	31.30	637.30	0.823	865	TMB
124TMB	1.07	0.750	240.35	65.4	0.49	0.73	6740	−8.50002	2.98227	−6.02665	3.51307	32.32	649.10	0.771	876	
123TMB	0.508	0.350	240.35	69.0	0.52	0.74	6810	−8.44191	2.92198	−5.66712	2.28086	34.55	664.50	0.875	894	
Napht	0.122	0.16	128.17	31	0.44	0.76	7070	−7.85178	2.17172	−3.70504	−4.81238	40.53	748.7	0.754	1162	NAPH
1 MNapht	0.192	0.22	142.2	25	0.32	0.7	6340	−7.5639	1.19577	−3.3813	−2.86388	35.66	772.3	3.067	1020	
2 MNapht	0.263	0.31	142.2	24.6	0.31	0.7	6320	−8.43595	2.88433	−5.70017	2.5089	35.05	761.4	3.067	1006	
nC7	0.4	0.669	100.2	3.4	0.06	0.72	6770	−7.67468	1.37068	−3.5362	−3.20243	27.32	540.1	0.395	680	nC79
nC8	0.8	1.173	114.2	0.7	0.01	0.66	6180	−7.87687	1.32514	−3.78494	−4.44565	24.82	568.81	0.511	699	
nC9	3.5	4.571	128.3	0.2	0.003	0.61	5750	−8.2448	1.57885	−4.38155	−4.04412	23.1	594.6	0.672	714	
nC10	14	16.484	142.3	0.1	0.001	0.57	5370	−8.56523	1.97756	−5.81971	−0.29982	21.07	617.6	0.862	727	nC1014
nC11	22.1	23.6	156.3	0	0	0.54	5030	−9.66	2.12	−6.18	−0.11	19.8	639	1.1	752	
nC12	21.7	21.345	170.34	0	0	0.5	4725	−8.6543	1.7061	−3.8448	−6.487	18.23	659.5	1.39	755.1	
nC13-14	25.53	22.355	191.35	0	0	0.46	4310	−8.867	1.3435	−3.9625	−7.3495	15.9	693.5	1.92	760.8	
nC15-16	7.9	6.032	219.45	0	0	0.41	4050	−9.3718	1.933	−5.3984	−6.3172	14.04	722.6	2.8	770.9	nC1518
nC17-18	1	0.675	247.98	0	0	0.39	3990	−8.7686	−0.9202	−1.7413	−13.4163	12.52	748.7	3.61	782.4	

The sequence of LNAPL remediation methods applied at this well is shown in Fig. 3. The overall field trial ran for 78 days and included LNAPL multi-phase recovery technologies such as skimming and vacuum-enhanced skimming with and without water table drawdown. Slurping was also tested (without water table drawdown). For vacuum-enhanced recovery, an average −4 kPa pressure (with an increasing trend) was applied in the capped well. For the water table drawdown technique, 47 m^3/day of water was pumped from beneath the LNAPL in the well. During the skimming phases, the skimmer elevation was manoeuvred at the LNAPL/water interface. For the slurping phase, a 25 mm stainless steel straw was lowered in the well to the approximate level of the air-liquid interface. The average in-well suction during the combined three-phase slurping was −2.2 kPa. Skimming was repeated as a control technique between applications of other techniques. This was to account for any changes in the rates due to mass removal from previous tests. Recovered LNAPL volumes were measured routinely and gas was sampled from air extraction lines to determine additional mass removal due to volatilisation and to determine compositional changes over time

Fig. 4 depicts the key trends over the complete period of the field trial; showing changes in the volume of the recovered LNAPL induced by application of each LNAPL recovery technique. A total of 5221 L of LNAPL was recovered over the period of the field trial, which is equivalent to removing the entire LNAPL volume initially in the aquifer within a 4.7 m radius of the primary recovery well. Initially, during skimming alone the rate of LNAPL recovery was of the order of 5–6 mL/s, but rapidly decreased to below 1 mL/s

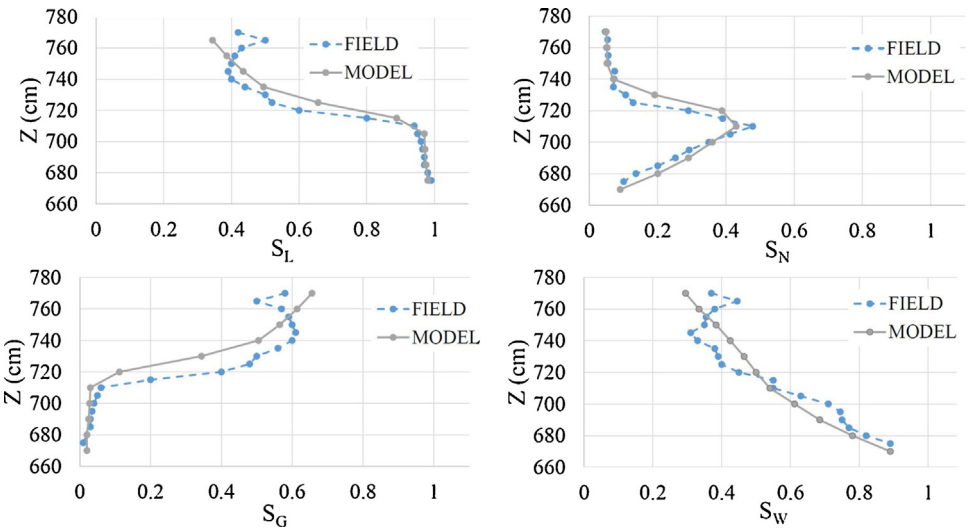

Fig. 2. The measured fluid saturations in the field (blue) and the initial conditions established in the model (grey). SL = liquid saturation, S_G = gas saturation, S_N = LNAPL saturation and S_W = water saturation. (For interpretation of the references to colour in this figure legend, the reader is referred to the web version of this article.)

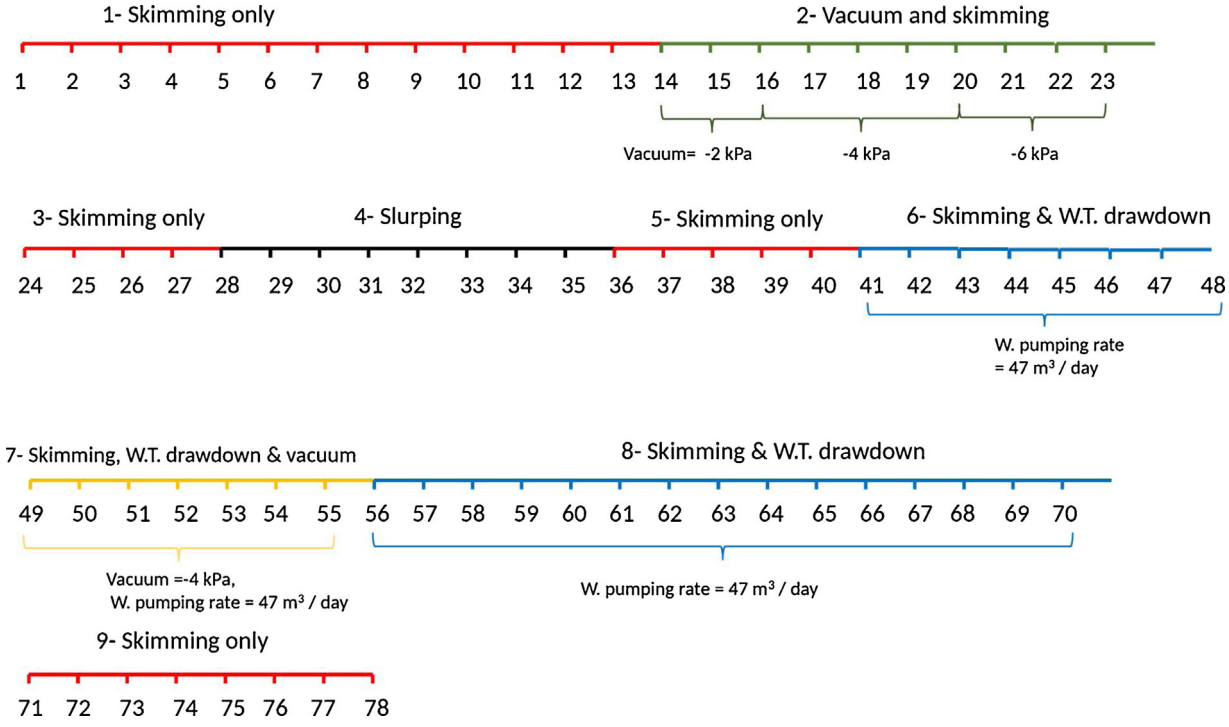

Fig. 3. The schedule of the recovery methods applied. Nine phases of remediation are depicted spanning 78 days. W.T = water table.

within the first few days. The initial high recovery was due to the abundance of mobile LNAPL in the near-radius of the well. Over nearly two weeks of skimming this rate remained almost constant. The sizable nature of the LNAPL plume and the intrinsic permeability of the aquifer [34] are thought to be the primary aspects that allow this recoverability. By applying an increasing vacuum whilst skimming (after day 14), the LNAPL recovery rate increased up to 1.6 mL/s. Some observed variability is due pump failures, such as the decrease on day 19. From day 20 onwards the rate of LNAPL recovery by vacuum-enhanced skimming decreased slightly to the end of the period, indicating the start of some limitations to LNAPL availability. Application of a vacuum would accelerate evaporation of more volatile compounds from LNAPL in the vicinity of the well, and lead to a decrease in LNAPL saturation which diminishes LNAPL mobility. Over these two periods 1643 L was recovered.

From day 24 for a duration of 4 days and also from day 36 for a duration of 5 days a skimming only approach was also applied. Volumes recovered over these periods were 51 L and 63 L respectively with average near-constant recovery rates of 0.14-0.15 mL/s. This was considerably less than the first phase of skimming (days 1–14) mainly due to the reduced LNAPL mobility around the well caused by mass loss during the vacuum-enhanced recovery. For the slurping phase (days 28–35), the rate of recovery was not able to be routinely measured, but the total volume of the recovered LNAPL was estimated as 426 L giving an average of 0.7 mL/s over this period.

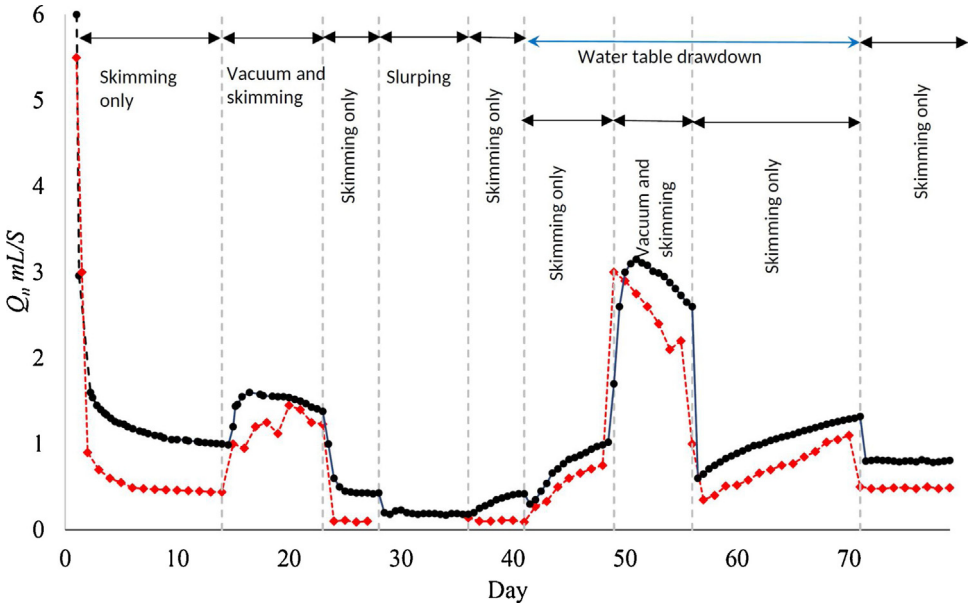

Fig. 4. LNAPL recovery rate in the field (red squares) and the simulation (black circles). (For interpretation of the references to colour in this figure legend, the reader is referred to the web version of this article.)

Drawing down the water table increased the hydraulic heads and the LNAPL gradient towards the well. This is observed from day 41–49 when the recovery rate continued to increase up to 0.81 mL/s recovering a total of 356 L of LNAPL over the period. Applying a vacuum on day 49 induced a peak rate of LNAPL recovery of about 3 mL/s, decreasing to 2.3 mL/s at the end of the period. This is clearly the highest rates of recovery induced over the trial after the first day or so, and in total extracted 1390 L of LNAPL over the 7 day period. We note that the magnitude of the decrease in the LNAPL recovery rate in this phase (3–2.3 mL/s) was higher than the recovery rate decrease (1.6–1.4 mL/s) in the first phase of vacuum-enhanced recovery (days 20–23). As discussed the enhanced volatilisation of compounds and the consequent decrease in LNAPL mobility around the well causes decreases in the rate of recovery such as these. Here, although the drawdown of the water table would enhance LNAPL mobility towards the well, it also redistributes LNAPL vertically and exposes a greater surface area of the LNAPL to the air. Overall, this enhances volatilisation and decreases LNAPL saturation and mobility.

Interestingly despite the significant total recovery of LNAPL to this point (almost 4000 L) in the field trial and the induced volatilisation of LNAPL, the rate of LNAPL recovery upon turning the vacuum off at day 56 was 0.3 mL/s and increased over the period of the phase at day 70 to a rate of 1.1 mL/s; recovering another 947 L of LNAPL over the period. Groundwater pumping to induce water table drawdown clearly had a strong effect on generating hydraulic and LNAPL gradients towards the well to allow successive recovery of such large volumes of LNAPL despite other processes driving redistribution and partitioning processes that would lead to reduced mobility and recoverability of the LNAPL. These are the complex multi-phase redistribution and partitioning processes that we have sought to model here accounting for the relevant level of representation of the field scale trials.

3. Governing equations and the representative model

The core model (TMVOC-MP) is based on two critical assumptions, (i) a Darcy flow regime prevails, and (ii) for partitioning, the model assumes equilibrium conditions in the form of Raoult's and Henry's Law between the three phases [22]. Both assumptions have been extensively examined and verified for meso and large (field)-scale problems [24,21,16]. In an integral form, the mass conservation equation is

$$\frac{d}{dt}\int_{V_n} M^K dV_n = \int_{\Gamma_n} \mathrm{F}^K \cdot \mathrm{n} d\Gamma_n + \int_{V_n} q^K dV_n \tag{1}$$

where dVn is an arbitrary subdomain, Γ_n is the surface of the subdomain, M^K is the mass of the component under study, F is the mass flux, q is the sink/source term (here indicating LNAPL, air and water extraction from the well) and n is the normal vector on the surface element. No chemical or biological reaction was considered here. This is justified as the duration of the field trial was relatively short (less than 100 days) compared to over a decade since the release at the site. Furthermore, $K = 1, \ldots, NK$, where NK is the number of components in the system. The advective mass flux is

$$\mathrm{F}^K = \sum_\beta X_\beta \mathrm{F}_\beta \tag{2}$$

where

$$\mathrm{F}_\beta = -k\frac{k_{r\beta}\rho_\beta}{\mu_\beta}\left(\nabla P_\beta - \rho_\beta \mathrm{g}\right) \tag{3}$$

and X_β is the molar fraction of K in phase β. In the above equation, k and $k_{r\beta}$ are the absolute and relative permeability (to phase β), μ is the dynamic viscosity and P is the total pressure. The vector g is gravitational acceleration. The feasibility of these equations for simulation of Darcy-scale interfacial mass transfer has been extensively verified in recent analytical, numerical and experimental studies [35,24,21,16]. Relative permeability and capillary pressure functions defined in [36] are applied. These include a van Genuchten-Mualem formulation. For the capillary head h [L],

$$\frac{S_j^{ij} - S_m}{1 - S_m} = \left[1 + \left(\alpha_{ij} h\right)^n\right]^{-m}, i, j = G, Aq, N, i \neq j \tag{4}$$

where S_j^{ij} is the effective wetting phase fluid saturation and S_m is the irreducible saturation of the wetting phase. The soil type in the LNAPL recovery field trial was sand [27,28] (we considered an absolute permeability of 5.0×10^{-12} m^2 [34,37]). Preliminary simulations showed that the site condition could fairly be assumed as

homogeneous and isotropic. The parameters n, α_{GN} and α_{AqN} were set to 1.84, 10 (m^{-1}) and 11 (m^{-1}) respectively [36,21]. Despite the site conditions (including the position of the recovery well, the LNAPL distribution and the soil) allowing a 2D radial coordinate simulation, we chose to conduct 3D simulations to reveal the features, capabilities and computational costs of the modelling framework in simulating complex field-scale problems with similar compositional and numerical mesh intensity. We also select this particular LNAPL remediation trial to verify the model as it covers a comprehensive and wide range of multi-phase LNAPL recovery approaches [27,28].

We categorised the components found in LNAPL from the site (Table 1) into nine representative groups. Indeed, compounds with similar thermo-physical and chemical properties are grouped together. This approach has been tested and verified in e.g., [21] and [16]. The representative groups in this study plus their average critical thermo-physical properties and abundance are introduced in Table 2.

A sketch of the simulation domain and the boundary conditions is shown in Fig. 1 (Left). In order to prepare the unstructured voronoi mesh required, we used WinGridder, which is a Windows-based graphical mesh generator for TOUGH group of codes [38]. A number of 180700 cells were generated to construct a cubic domain 100 m × 100 m in plan and 10 m in depth (including 100 evenly distributed mesh layers). The well was located at the centre of the domain. Dirichlet boundary conditions are imposed at the outer boundaries.[3] Fig. 5 shows the mesh at three different scales. The cells representing the well wall are marked in the red ring in the right subfigure.

4. Code performance

Two scientific computing facilities were used. The first system was the Magnus Cray XC40 supercomputer (Intel Xeon Haswell processor cores) located at the Pawsey Supercomputing Centre in Perth, Australia. Each node in this machine consists of 24 cores. The second system was the CSIRO Pearcey cluster which is a Dell PowerEdge M630 cluster system running Linux. Each node has dual 10 core Intel Xeon E5-2660 V3 processors. The entire simulations were finished using almost 10^5 and 0.85 million CPU-hours on Magnus and Pearcey respectively. All the simulations here were identically conducted on both systems and showed close agreement with less than 1% difference in the simulated LNAPL recovery rates. The performance of the systems used for different stages of the simulations is depicted in Fig. 6.

In subfigures A-C, the performance of the Magnus supercomputer in establishing the initial water table conditions (with no NAPL) is shown. The number of time steps in these test simulations is 500 representing 512×10^3 s of simulation time. As both real-time and computational cost mattered on Magnus, a number of 28 Nodes (672 processors) were selected for this phase. Subfigure D compares the wall-time required by Magnus and Pearcey to conduct almost two hours of simulation of early stages of skimming and water table drawdown in which the system was very dynamic and therefore, the time steps were shorter (almost 120 time steps to cover the two hours of the simulation time). The horizontal coordinate in this subfigure shows the number of cores used (Note Magnus has 24 cores in each node and Pearcey has 20). It is seen that the optimum number of cores in Pearcey for the transient part of the simulations is around 200. The increase in the required wall-time for cores above this is due to the accumulated communication time between the processors. On the other hand, the wall-time trend on Magnus were decreasing for up to the maximum number of the CPUs we used (720). It was also noted that for the equal number of cores and the transient simulations including all the eleven compounds (nine representative groups, water and air), Magnus was at least seven times faster than Pearcey which is potentially due to its advanced architecture.

5. Simulation, results and discussion

The first step was to establish the appropriate water table conditions with two compounds (air and water). This is a standard approach in TMVOC and has been discussed e.g., in [24]. Then the measured initial depth-wise LNAPL saturation profile was reconstructed. The final profile shown in Fig. 2 remained stable and approximated the soil core measurements, allowing testing of the model for recovery options. As the extent of the LNAPL plume at the site was not exactly known, we assumed that it occupied the entire domain (plan view). The side-domain boundary conditions were Dirichlet, the bottom was no-flow and the surface boundary condition, except the well cap, was held at a constant atmospheric pressure. Once the MESH file was generated with WinGridder, a separate Matlab script was developed and used to read it and to identify the cells representing the side boundaries, the well cap, the well side-isolations (casing), the coarse sand layer surrounding the bottom-half of the well and the inside-well domain. The MESH file was then updated with different ROCK names for these mentioned domains. The no-flow boundary condition was imposed at the well cap and for the casing. The absolute permeability for the coarse sand layer was not measured in the field and we repeated a number of simulations with 10^{-9} m^2 and 10^{-10} m^2 [37]. As the results did not show considerable difference (indeed this value was not the limiting parameter for the LNAPL transport) we set it to 10^{-9} m^2 which also aided numerical convergence.

For the skimming technique, the cells located inside the well domain with the highest value of LNAPL saturation were identified and were used as the elevation of LNAPL extraction. These cells raised and fell for the case of vacuum-enhanced skimming and skimming with water table drawdown respectively. This had also been reported in the field measurements (the fluid interfaces). For the vacuum-enhanced recovery and water table drawdown, separate sink cells (for gas and water) were defined at the top and bottom of the well respectively.

Simulated results for LNAPL recovery rates over the 78 days of the field trial compared to field measurements are shown in Fig. 4. Despite uncertainties in the geo-mechanical and hydro-geological features of the site, as well as the LNAPL distribution, it is seen that the model reproduces all the main trends in the LNAPL recovery rate over each phase of the sequential application of the LNAPL remediation methods at the site. The simulated results in general overpredict the recovery rates for most of the phases of recovery but for each phase the simulations mimic decreasing or increasing trends in rates. No attempt was made to adjust parameters further to overlay simulation and field data since trends and absolute rates were comparable. The aim was to be able to simulate trends within reasonable accuracy and magnitude. Even though the field trial was over a limited period, overprediction of rates via the simulation, may be because other mass removal processes are not turned on in the simulation (such as biodegradation processes). Some biodegradation was observed to occur at the field site [27].

The comparable trends simulated by the framework shows a considerable robustness within the framework and code; as it requires switching between a period dominated by LNAPL mobility, to one where air movement and volatilisation are induced, to one where water pumping and drawdown accompanying all other processes. These are critical to accommodate in the code and rep-

[3] Other option is transient infinite elements which is not currently available in TMVOC-MP [39].

Table 2
Fraction of the representative groups in the simulated LNAPL plus their mole-averaged vapour pressure (V. pres.) and water solubility.

	M_W	Mole%	Mass%	V. Press (*Pa*)	Solubility (*mole/mole*)
BEN	78.11	0.062	0.029	1.26×10^4	40.6×10^{-5}
TOL	92.14	0.002	0.001	3.79×10^3	10.69×10^{-5}
XYL	106.16	0.592	0.375	1.14×10^3	2.91×10^{-5}
ETB	106.17	0.35	0.223	1.28×10^3	3.12×10^{-5}
TMB	240.35	1.3	1.865	277	0.48×10^{-5}
NAPH	138.98	0.79	0.577	12.68	0.34×10^{-5}
nC79	122.79	6.412	4.7	934.42	0.01×10^{-5}
nC1014	166.46	84.134	83.33	27.66	0
nC1518	222.32	6.708	8.9	0.55	0

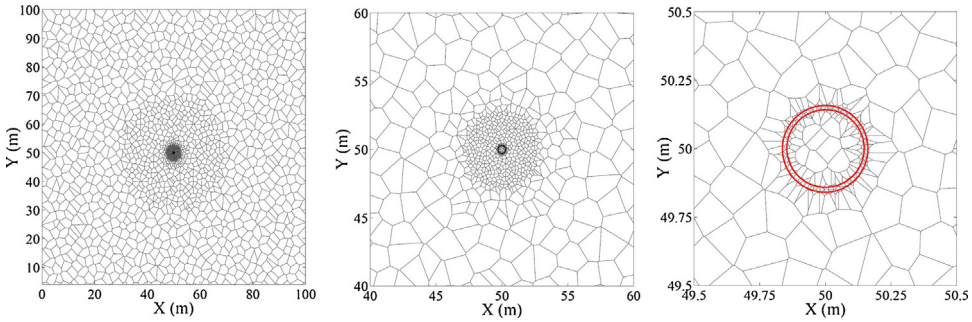

Fig. 5. The voronoi mesh used (plan view) for the study at three different zooms. The cells representing the well wall are marked in the red ring in the right subfigure. (For interpretation of the references to colour in this figure legend, the reader is referred to the web version of this article.)

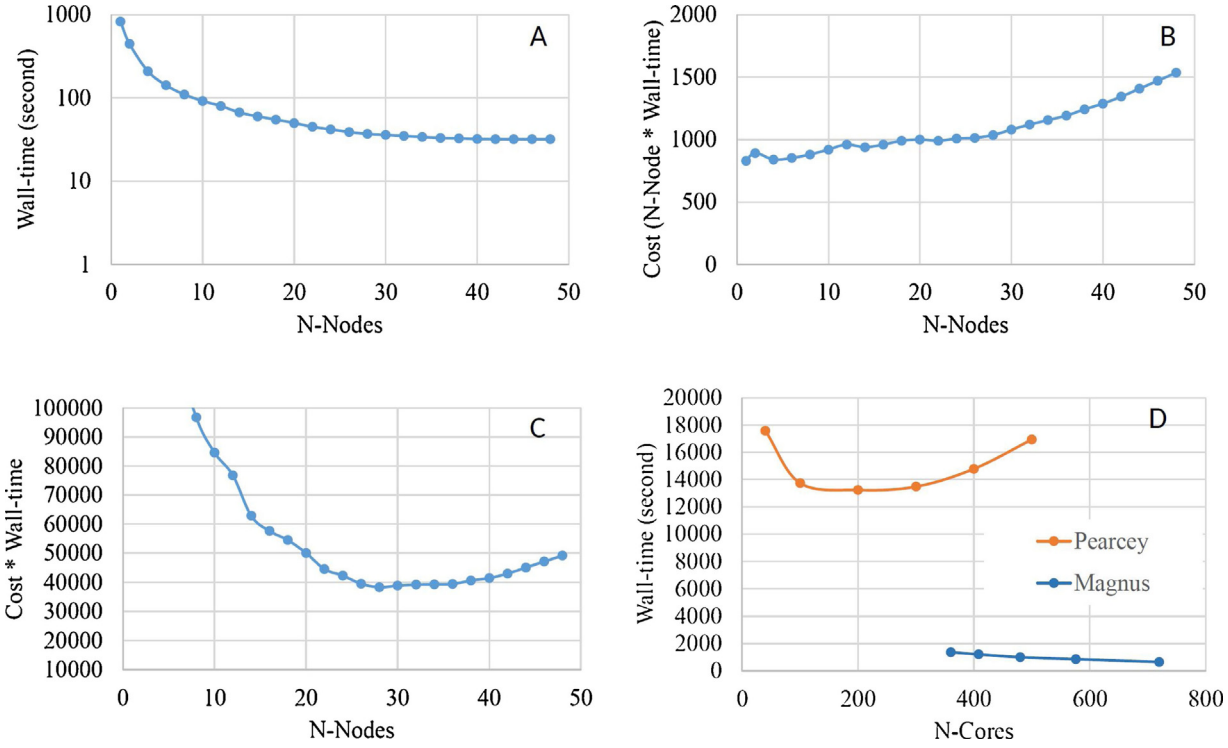

Fig. 6. Performance of the Cray supercomputer for the initial conditions establishment stage (A-C) and comparison of the Magnus supercomputer and Pearcey cluster for the skimming and water table drawdown stage (D).

resent adequately. The code is shown to be adequate for liquid phase recovery while accounting for volatilisation, water flows and reasonable dissolution processes as well.

Beyond LNAPL mass recovery from the subsurface, regulation demands attention to components of LNAPLs that are drivers of risk at contaminated sites (such as benzene) and their partitioning to groundwater and soil gas phases (for example for vapour intrusion assessment). Such partitioning of hazardous chemicals in different phases is critical to the determination of LNAPL recovery endpoints and closure risk assessment. Therefore, a representative simulation should adequately address the presence and partitioning of critical compounds in the subsurface.

To evaluate the framework for this aspect, simulated results were determined for the initial vacuum-enhanced LNAPL recovery phase of the field trial (days 14–20 on Fig. 3) where data are available for the concentration of BTEX (benzene, toluene, ethylbenzene

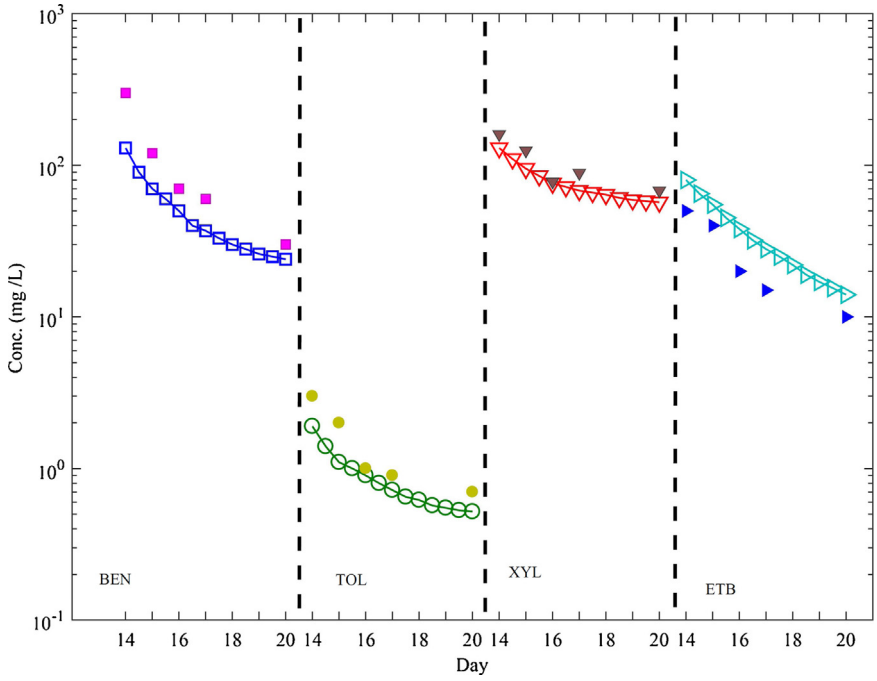

Fig. 7. Concentration of various compounds in the soil gas during the initial vacuum-enhanced recovery. Individual points are field measurements and the lines with symbols are the simulations.

and xylene) compounds measured in the extracted soil gas. A comparison of the simulation and field data is shown in Fig. 7. Note the very low concentrations for toluene were due to its initially very low molar fraction in the LNAPL (Table 2). Despite the lower molar fraction of benzene in the LNAPL compared to xylene and ethylbenzene, benzene has a significantly higher vapour pressure [24] which yielded a higher concentration for benzene initially in the extracted gaseous phase. Concentrations of each of the BTEX compounds decreased over time. The decreasing concentrations are due to the near-well depletion of volatile compounds in the LNAPL and as the time proceeds, the molar fraction of these compounds decreases adjacent to the well. This is also evidence for the declining LNAPL recovery rates in the field when including vacuum-enhanced recovery (Fig. 3).

It is observed in Fig. 7 that the model is able to predict values and trends in the concentration changes over time and the proportionality of different compounds in the gas phase, even for a low abundance compound in the LNAPL like toluene (less than 10^{-2}% by mole-see Table 1). Simulations underestimate benzene concentrations (by a factor of approximately 1.2–2.5) whereas the code overpredicts ethylbenzene concentrations slightly. This is good agreement, given other uncertainties and processes governing the extracted gas concentration [23], such as parameter estimates and variations and aquifer heterogeneity. Overall, this shows an additional powerful but essential attribute of the simulation framework with respect to enabling the incorporation of risk assessment associated with the partitioning and transport of hazardous chemicals in different phases.

The radius of influence of the vacuum applied to the well is seen in Fig. 8 where the concentration distribution of various compounds in the simulation is depicted for day 23. A separate Matlab script had to be prepared to read the MESH and modified SAVE file (see the Appendix A) and produce the figure. It is observed that during vacuum-enhanced skimming, the radius of influence of the well with respect to soil vapours is almost 15 m. This is consistent with the field measurements, where the soil gas pressure around the well was monitored in observation and multi-level wells during the vacuum-enhanced recovery. Also note the concentration scale for toluene is almost two orders of magnitude less than the counterpart values for benzene, xylene and ethylbenzene. As discussed, this is due to the very low initial molar fraction of toluene in the LNAPL phase (Table 1).

So far, we have shown that within a reasonable computational time, it is possible to simulate 3D site-scale multi-phase LNAPL remediation approaches and determine risks associated with various hazardous compounds in different phases. This is of particular importance because field LNAPL recovery and remediation problems may include thousands of chemicals in the LNAPL, heterogeneity in the soil and the LNAPL plume, complexity in the recovery well configurations, number of the recovery wells and additionally the groundwater flow. It has also been shown that rarely is a LNAPL plume symmetrical and therefore a 2D simulation strategy may be misleading or not representative enough [24]. Consequently, determination of an endpoint for costly recovery techniques may be a challenging task sometimes requiring 3D multi-phase and multi-component simulations to avoid unnecessary extensions to field-based remedial efforts.

The study here provides an indicative estimate of the computational resources required to representatively simulate field-scale processes. It provides a basis to trade-off accuracy with system complexity. The framework was validated over the relatively complex but short 78 day trial and enables longer term prediction of the effectiveness of remedial technologies in achieving mass removal but also determining the risk profile of hazardous chemicals once a recovery endpoint is reached. The field data and the computational results are applicable for future model verifications including development and application of alternate and possibly simpler approaches. Technical features on how to adopt the code for supercomputing facilities are provided in the Appendix A.

6. Conclusions

We reported results of a LNAPL remediation field trial (including sequential application of various multi-phase LNAPL recovery approaches) and used the data to validate a new simulation framework (including some pre- and post-processing codes for

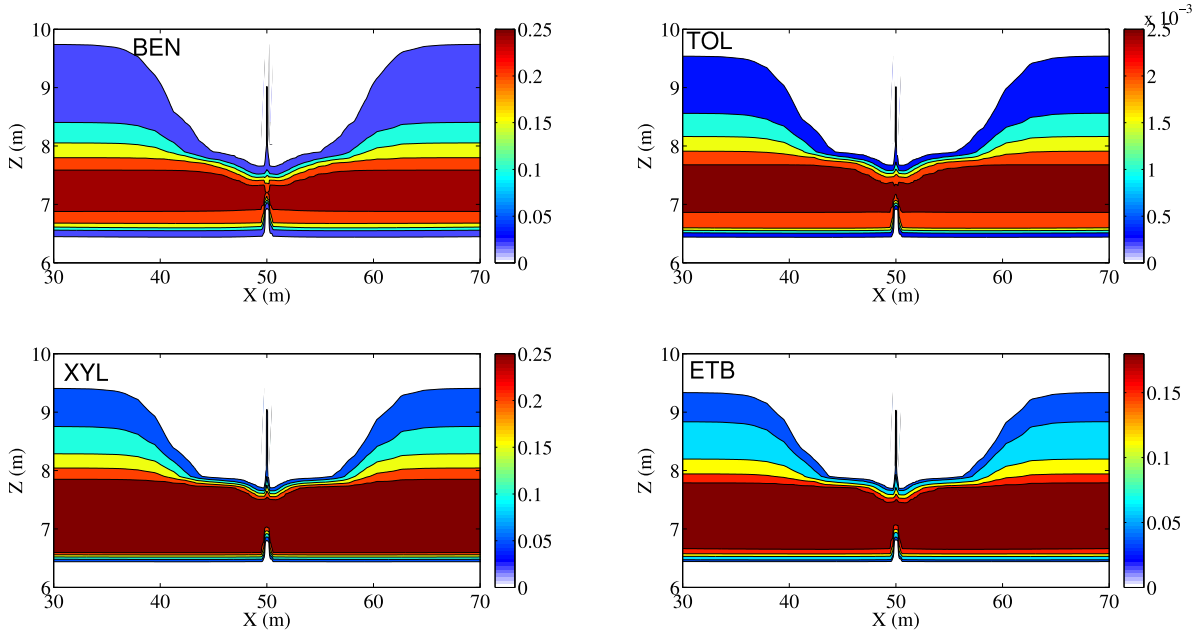

Fig. 8. Contours of the BTEX concentration (g/m3) in the soil gas at the end of the vacuum-enhanced recovery.

TMVOC-MP) to model complex LNAPL recovery methods at field time and length scales. To achieve this, beyond multi-phase considerations, multi-component partitioning and transport were accommodated for the first time for LNAPL recovery and subsurface remediation techniques. We evaluated the framework on two different high-performance computing facilities and verified it against the reported case-study including a sequence of various LNAPL remedial approaches. We intentionally kept the three dimensional layout of the problem to test the ability and feasibility of the framework for simulating asymmetric field-size problems using similar computational resources (albeit not considered in this paper). We also considered LNAPL as a multi-component mixture comprising nine representative groups for various aromatics and alkanes to also include partitioning of the hazardous compounds in different phases, changes to the remaining LNAPL physical and chemical properties as well as to test the model with respect to mimicking the measured concentrations of hazardous chemicals determined during remedial efforts.

Having appropriate computational resources available (e.g., similar those used here), allows construction of a framework based on TMVOC-MP which can help to assess the effectiveness of complex subsurface and LNAPL remedial and recovery methods under various site conditions. This is critical to enable longer time-frame simulations (decades to centuries) to determine the effective endpoint of LNAPL recovery/remediation methods, as well as provide compound-specific data that informs risk assessments associated with various hazardous chemicals for possible site closure decisions. As TMVOC-MP is available with its source code, it is also possible to modify the code to include new features that represent additional field-scale processes in the parallel version (e.g. hysteresis as in [21], biodegradation kinetics [40] and recent understandings regarding the effects of soil compressibility and non-isothermal conditions [41,18,42]).

Acknowledgments

The work has been supported by the Cooperative Research Centre for Contamination Assessment and Remediation of the Environment (CRC CARE), whose activities are funded by the Australian Government's Cooperative Research Centres Programme. It was also supported by resources provided by the Pawsey Supercomputing Centre with funding from the Australian Government and the Government of Western Australia and also the resources at CSIRO Pearcey cluster. Technical help from Paul Ryan for compiling TMVOC-MP on Pearcey is acknowledged.

Appendix A.

Some of the technical insights for compiling the TMVOC-MP code and running the simulations are shared here. The authors were not able to print sink and source generation information in GOFT (It seems that this section is not parallelised). Instead, an indirect approach was used. The fluid flow values in COFT for each desired sink/source were summed (for all the connections and considering the signs) and the effect of changes in the saturation (in FOFT) were included. Using this approach and knowing that the FLO values in COFT are in moles/s, it was noticed that the entries in the INFILE-GENER have the same values. Another issue the authors experienced was with respect to the format of 8-character elements in the SAVE file. Indeed, the authors needed to prepare a separate Matlab script to convert the incomplete elements names in the SAVE file to the correct format and then use it as INCON (if needed). The authors were unable to compile the codes with the default Metis and Aztec libraries installed on the machines. Aztec 2.1 and Metis-4.0.3 were compiled separately and the resulting libmetis.a and libaztec.a libiraries were used to compile the code. In contrast with the system using MPICH, the system using OpenMPI encountered some difficulties in compiling the code. In particular, changes had to be applied to synchronize the value for MPI-COMM-WORLD in Fortran and C (for the libraries used).

References

[1] K. Sookhak Lari, H. Safavi, A simulation-optimization model for 'Air Sparging' and 'Pump and Treat' groundwater remediation technologies, J. Environ. Inform. 12 (2008) 44–53.
[2] G.B. Davis, B.M. Patterson, M.G. Trefry, Evidence for instantaneous oxygen limited biodegradation of petroleum hydrocarbon vapors in the subsurface, Groundwater Monit. Remediat. 29 (2009) 126–137.
[3] G.B. Davis, J.L. Rayner, M.G. Trefry, S.J. Fisher, B.M. Patterson, Measurement and modeling of temporal variations in hydrocarbon vapor behaviour in a layered soil profile, Vadose Zone J. 4 (2005) 225–239.

[4] D.A. Lang, T.P. Bastow, B. van Aarssen, B. Warton, G.B. Davis, C.D. Johnston, Polar compounds from the dissolution of weathered diesel, Groundwater Monit. Remediat. 29 (2009) 85–93.
[5] G. Lekmine, T.P. Bastow, C.D. Johnston, G.B. Davis, Dissolution of multi-component LNAPL gasolines: the effects of weathering and composition, J. Contam. Hydrol. 160 (2014) 1–11.
[6] M.O. Rivett, G.P. Wealthall, R.A. Dearden, T.A. McAlary, Review of unsaturated-zone transport and attenuation of volatile organic compound (VOC) plumes leached from shallow source zones, J. Contam. Hydrol. 123 (2011) 130–156.
[7] G.B. Davis, C.D. Johnston, B.M. Patterson, C. Barber, M. Bennett, Estimation of biodegradation rates using respiration tests during in situ bioremediation of weathered diesel NAPL, Groundwater Monit. Remediat. 18 (1998) 123–132.
[8] C.D. Johnston, J.L. Rayner, D. Briegel, Effectiveness of in situ air sparging for removing NAPL gasoline from a sandy aquifer near Perth, Western Australia, J. Contam. Hydrol. 59 (2002) 87–111.
[9] F.I. Khan, T. Husain, R. Hejazi, An overview and analysis of site remediation technologies, J. Environ. Manag. 71 (2004) 95–122.
[10] G.B. Davis, D. Laslett, B.M. Patterson, C.D. Johnston, Integrating spatial and temporal oxygen data to improve the quantification of in situ petroleum biodegradation rates, J. Environ. Manag. 117 (2013) 42–49.
[11] C. Zhao, B. Hobbs, A. Ord, Fundamentals of Computational Geoscience: Numerical Methods and Algorithms, Springer, 2009.
[12] H. Prommer, D.A. Barry, G.B. Davis, Numerical modelling for design and evaluation of groundwater remediation schemes, Ecol. Modell. 128 (2000) 181–195.
[13] M.M. de Souza, M. Oostrom, M.D. White, G.C. da Silva Jr., M.C. Barbosa, Simulation of subsurface multiphase contaminant extraction using a BioslurpingWell model, Transp. Porous Media 114 (2016) 649–673.
[14] C.D. Johnston, M.G. Trefry, Characteristics of light nonaqueous phase liquid recovery in the presence of fine-scale soil layering, Water Resour. Res. 45 (2009) W05412.
[15] M. Vasudevan, C.D. Johnston, T.P. Bastow, G. Lekmine, J.L. Rayner, I. Nambi, G. Suresh Kumar, R. Ravi Krishna, G.B. Davis, Effect of compositional heterogeneity on dissolution of non-ideal LNAPL mixtures, J. Contam. Hydrol. 194 (2016) 10–16.
[16] G. Lekmine, K. Sookhak Lari, C.D. Johnston, T.P. Bastow, J.L. Rayner, G.B. Davis, Evaluating the reliability of equilibrium dissolution assumption from residual gasoline in contact with water saturated sands, J. Contam. Hydrol. 196 (2017) 30–42.
[17] C. Zhao, B.E. Hobbs, A. Ord, Theoretical analyses of nonaqueous phase liquid dissolution-induced instability in two-dimensional fluid-saturated porous media, Int. J. Numer. Anal. Methods Geomech. 34 (2010) 1767–1796.
[18] C. Zhao, B.E. Hobbs, A. Ord, Theoretical analyses of chemical dissolution-front instability in fluid-saturated porous media under non-isothermal conditions, Int. J. Numer. Anal. Methods Geomech. 39 (2015) 799–820.
[19] Q. Yang, Y. Li, J. Zhou, X. Xie, Y. Su, Q. Gu, M. Kamon, Modelling of benzene distribution in the subsurface of an abandoned gas plant site after a long term of groundwater table fluctuation, Huydrol. Processes 27 (2013) 3217–3226.
[20] R.W. Falta, B.H. Kueper, Modeling Plume Responses To Source Treatment, 2014.
[21] K. Sookhak Lari, G.B. Davis, C.D. Johnston, Incorporating hysteresis in a multi-phase multi-component NAPL modelling framework; a multi-component LNAPL gasoline example, Adv. Water Resour. 96 (2016) 190–201.
[22] K. Pruess, A. Battistelli, TMVOC, A Numerical Simulator for Three-Phase Non-isothermal Flows of Multicomponent Hydrocarbon Mixtures in Saturated-Unsaturated Heterogeneous Media, Lawrence Berkeley National Laboratory, Berkeley, CA 94720 U.S.A., 2002.
[23] K. Sookhak Lari, J.L. Rayner, G.B. Davis, A computational assessment of representative sampling of soil gas using existing groundwater monitoring wells screened across the water table, J. Hazard. Mater. 335 (2017) 197–207, http://dx.doi.org/10.1016/j.jhazmat.2017.04.006.
[24] K. Sookhak Lari, C.D. Johnston, G.B. Davis, Gasoline multi-phase and multi-component partitioning in the vadose zone: dynamics and risk longevity, Vadose Zone J. 15 (3) (2016) 1–15, http://dx.doi.org/10.2136/vzj2015.07.0100.
[25] K. Zhang, H. Yamamoto, K. Pruess, TMVOC-MP: A Parallel Numerical Simulator for ThreePhase Non-isothermal Flows of Multicomponent Hydrocarbon Mixtures in Porous/Fractured Media Tech. Rep., Lawrence Berkeley National Laboratory, 2007.
[26] R.W. Falta, B.H. Kueper, Modeling plume responses to source treatment Chlorinated Solvent Source Zone Remediation, 145–186, Springer, 2014.
[27] C.D. Johnston, S. Fisher, J.L. Rayner, Removal of Petroleum Hydrocarbons from the Vadose Zone During Multi-phase Extraction at a Contaminated Industrial Site, Groundwater Quality: Natural and Enhanced Restoration of Groundwater Pollution (Proceedings of the Groundwater Quality 2001 Conference, Sheffield,UK), IAHS, 2002, pp. 287–293.
[28] C.D. Johnston, Selecting and assessing strategies for remediating LNAPL in soils and aquifers, in: Technical Report 18, CRC CARE, Adelaide Australia, 2010.
[29] C.D. Johnston, S.J. Fisher, N.L. Innes, J.L. Rayner, Field Evidence for Biodegradation of Petroleum Hydrocarbons During Multi-phase Extraction, Proceedings of the 3rd European Bioremediation Conference, Chania, 2005 (p. 019).
[30] Rainfall WATER CORPORATION, 2017 (URL) www.watercorporation.com.au/water-supply/.
[31] J. McGarry, Correlation and prediction of the vapor pressures of pure liquids over large pressure ranges, Ind. Eng. Chem. Process Des. Dev. 22 (1983) 313–322.
[32] C.L. Yaws, Transport Properties of Chemicals and Hydrocarbons: Viscosity, Thermal Conductivity, and Diffusivity for More Than 7800 Hydrocarbons and Chemicals, Including C1 to C100 Organics and Ac to Zr Inorganics, William Andrew, 2009.
[33] D. Mackay, W.Y. Shiu, K.C. Ma, S.C. Lee, Handbook of Physical-Chemical Properties and Environmental Fate for Organic Chemicals, Taylor & Francis, 2006.
[34] R.F. Carsel, R.S. Parrish, Developing joint probability distributions of soil water retention characteristics, Water Resour. Res. 24 (1988) 755–769.
[35] K. Sookhak Lari, C.D. Johnston, G.B. Davis, Interfacial mass transport in porous media augmented with bulk reactions: analytical and numerical solutions, Transp. Porous Media 106 (2015) 405–423, http://dx.doi.org/10.1007/s11242-014-0407-3.
[36] J.C. Parker, R.J. Lenhard, T. Kuppusamy, A parametric model for constitutive properties governing multiphase flow in porous media, Water Resour. Res. 23 (1987) 618–624.
[37] M.J. Thoma, W. Barrash, M. Cardiff, J. Bradford, J. Mead, Estimating unsaturated hydraulic functions for coarse sediment from a field-scale infiltration experiment, Vadose Zone J. 13 (2014) 1–17.
[38] L. Pan, User Information Document for WINGRIDDER Version 3.0, Tech. Rep., U. S, Department of Energy, 2007.
[39] C. Zhao, Dynamic and Transient Infinite Elements: Theory and Geotechnical Geophysical, Springer Geoenvironmental Applications, 2009.
[40] C.D. Johnston, J.L. Rayner, B.M. Patterson, G.B. Davis, The contribution of volatilisation and biodegradation during air sparging of dissolved BTEX-contaminated groundwater, J. Contam. Hydrol. 33 (1998) 377–404.
[41] C. Zhao, B. Hobbs, A. Ord, Effects of medium and pore-fluid compressibility on chemical-dissolution front instability in fluid-saturated porous media, Int. J. Numer. Anal. Methods Geomch. 36 (2012) 1077–1100.
[42] C. Zhao, B.E. Hobbs, A. Ord, Computational simulation of chemical dissolution-front instability in fluid-saturated porous media under non-isothermal conditions, Int. J. Numer. Methods Eng. 102 (2015) 135–156.